Int. J. High Technology Ceramics **2** (1986) 179–193

The Effect of Post-Creep Thermal Treatment on Cavitation Damage

R. A. Page and J. Lankford

Southwest Research Institute, 6220 Culebra Rd, San Antonio, Texas 78284, USA

SUMMARY

Small-angle neutron scattering measurements have shown that nucleation and growth of grain boundary cavities occurs, in many ceramics, during the early stages of creep. Subsequent failure generally transpires by cavity coalescence to form cracks, followed by growth of the cracks. The effect on creep cavity populations of thermal treatment, both with and without pressure, has been investigated by comparing cavity distributions obtained from small-angle scattering measurements performed before and after the thermal treatments. The results of these measurements indicate that creep cavities can be removed if sufficient temperature and pressure are applied. From the results obtained on a sintered alumina and a hot-pressed silicon carbide, it appears that hydrostatic pressures approximately equal to the creep stress are required to afford substantial cavity sintering. The use of insufficient pressure not only fails to sinter the cavities formed during prior creep but has also been shown to lead to the nucleation of additional cavities, thus, apparently, increasing the level of damage.

1. INTRODUCTION

Creep failure of polycrystalline ceramics frequently occurs by grain boundary cavitation, which involves the individual processes of cavity nucleation, cavity growth, and cavity coalescence. The early stages of creep are generally dominated by cavity nucleation and growth. In this regime, increases in the number and/or size of cavities are responsible for reductions in the remaining creep life. Hence, if in some way the number and/or size of

Int. J. High Technology Ceramics 0267-3762/86/$03·50

cavities were reduced, one would expect to regain at least a significant portion of the lost lifetime.

The operative cavitation mechanism in ceramics is thought to vary with the grain boundary microstructure.[1] Ceramic systems with glass-free grain boundaries are thought to cavitate by diffusive growth, while a viscous mechanism has been postulated for systems that contain a glassy grain boundary phase. Examination of the pore growth theories suggests a means by which the pores may be removed. For diffusive growth, the rate of increase of cavity radius, $\dot{R}$, is approximately[2]

$$\dot{R} \sim \frac{2\pi D_g Z(\sigma_n - P - 2\gamma/R)\Omega S}{kTlR} \tag{1}$$

where D_g is the grain boundary diffusion coefficient, Z is the grain boundary thickness, Ω the atomic volume, l the cavity spacing, R the cavity radius, σ_n the normal stress on the grain boundary, P the hydrostatic pressure, γ the surface energy, k is Boltzman's constant, T is temperature, and S is approximately unity for expected values of R/l. For viscous growth, the rate of increase of cavity radius is given similarly by[3]

$$\dot{R} = \frac{(2\sqrt{3}l^2 - \beta\pi R^2)h^2[\sigma_n - 2\gamma_s K(1 - 0{\cdot}9\alpha^2)]}{12\pi\eta l^2 \beta R[0{\cdot}96\alpha - \ln\alpha - 0{\cdot}23\alpha^4 - 0{\cdot}72]} \tag{2}$$

where $\alpha = R/l$, β is a geometrical parameter equal to one for a penny-shaped cavity and two thirds for an oblate spheroid cavity, η and h are the viscosity and thickness, respectively, of the glassy phase, and

$$K = \frac{1}{R} + \frac{2}{h}\left[\frac{\gamma_b - \gamma_i}{\gamma_s}\right] \tag{3}$$

where γ_s, γ_b and γ_i are the energies of the glassy-film-free surface, the grain boundary, and the glassy film/grain boundary interface, respectively. It is evident from eqns (1) and (2) that in the absence of a normal traction across the grain boundary ($\sigma_n = 0$), the surface tension will act to sinter the cavities. Hence, the theory suggests that thermal hold periods with no applied load should provide a means by which the cavities can be reduced in size, if not totally eliminated. Additionally, the application of a hydrostatic pressure during the thermal treatment should accelerate cavity sintering.

This paper presents the results of a series of experiments designed to determine the extent of cavity sintering that can be expected during thermal hold periods at the creep temperature, both with and without an applied hydrostatic pressure. To evaluate fully cavity sintering it is necessary to determine both the size, or size distribution, and the number of cavities, and to do so with a large enough sample so that the results have statistical

significance. Small-angle neutron scattering (SANS) is the only technique presently available that can provide a statistically significant measure of both the number and the size of cavities, and it has been used successfully to characterize cavity distributions in metals[4-9] and ceramics,[10-12] arising from irradiation, fatigue, and creep. Hence, SANS was employed in the cavity characterizations performed in this study.

2. EXPERIMENTAL

2.1. Materials

Two materials were included in this study: a hot-pressed silicon carbide (NC 203, Norton Company, Worcester, MA, USA) and a sintered alumina (Lucalox, General Electric Lamp Glass Division, Cleveland, OH, USA). References 11 and 12 should be referred to for a detailed description of the microstructures of these two materials. Suffice it to say that the results of the previous characterizations indicated: (a) that the hot-pressed silicon carbide contained a thin, continuous grain boundary phase, it thus being representative of the liquid-phase sintered materials in which cavity growth is thought to occur by a viscous hole growth process; and (b) that the sintered alumina contained no glassy grain boundary phase, and was thus representative of the single-phase materials in which cavity growth is most likely a grain boundary diffusion process. Additionally, the microstructures of both materials were shown to be stable at the temperature employed for both creep and post-creep thermal treatment in this study.

2.2. Creep tests

Compression creep specimens were fabricated in the form of right-circular cylinders, 6·4 mm in diameter and 12·7 mm long. Creep testing was performed at 1600 °C in a servo-controlled hydraulic test machine equipped with a controlled environment (titanium-gettered argon) resistance furnace. The silicon carbide and alumina specimens were crept at compressive stresses of 570 and 140 MPa, respectively. The individual test durations are listed in Table 1. At the completion of each test the specimens were rapidly cooled to room temperature before being unloaded in order to freeze in the cavity distribution present at the test temperature.

A comparison of the effects of post-creep thermal treatment ideally should be performed on specimens with identical initial states of damage. Unfortunately, well-characterized specimens with identical creep strains were not available for these comparisons. However, it is believed that the

TABLE 1
Creep Conditions of Samples Examined

Sample number	*Material*	*Temperature/°C*	*Stress/MPa*	*Time/h*	*Creep strain*
A-1	Alumina	1 600	140	6·0	0·016 8
A-2	Alumina	1 600	140	8·8	0·033 8
A-3	Alumina	1 600	140	3·3	0·027 0
A-4	Alumina	1 600	140	3·5	0·028 0
S-1	Silicon carbide	1 600	570	25	0·018 7
S-2	Silicon carbide	1 600	570	37	0·018 9
S-3	Silicon carbide	1 600	570	12	0·007 98

variation in creep strain of the specimens employed in this study would not qualitatively affect the reported results.

2.3. SANS measurements

Rectangular flats, 5 mm × 12·7 mm, were ground and polished on opposite sides of the specimens following creep. This procedure yielded specimens approximately 3·7 mm thick, as measured between the parallel flats. Final polishing was performed such that grain pullout was minimized and a similar surface finish was achieved on each specimen.

The small-angle scattering measurements, which were performed on the 30-m instrument at the National Center for Small-Angle Scattering Research at Oak Ridge National Laboratory,[13] utilized an incident neutron wavelength, λ, of 0·475 nm, and sample to detector distances of 9 m and 16·5 m. This yielded intensity data at scattering vectors, $\mathbf{q}$, from 0·037 nm^{-1} to 0·2 nm^{-1}, where $\mathbf{q} = 4\pi \sin\theta/\lambda$ and 2θ is the scattering angle. Parasitic scattering effects arising from electronic background and the empty specimen holder, as well as non-uniform detector sensitivity, were corrected for as described in Reference 7. The corrected data were radially averaged and then converted to a macroscopic differential scattering cross-section, $d\Sigma/d\Omega$, by calibration in reference to the scattering cross-section of voids in a well-characterized irradiated aluminum sample.[4]

2.4. Post-creep thermal treatment

Following the SANS characterization of the creep cavity distribution, one sample of each material was held for 24 h at 1600 °C, the creep temperature, with no applied load, one sample of each material was held for 24 h at 1600 °C with an applied hydrostatic stress of 34 MPa, and one sample of

TABLE 2
Thermal Treatments

Sample number	*Material*	*Treatment conditions*		
		Temperature/°C	*Pressure/MPa*	*Time/h*
A-1	Alumina	1 600	—	24
A-2	Alumina	1 600	34	24
A-3	Alumina	1 600	240	4
A-4	Alumina	No thermal treatment performed		
S-1	Silicon carbide	1 600	—	24
S-2	Silicon carbide	1 600	34	24
S-3	Silicon carbide	1 600	240	4

each material was held for 4 h at 1600 °C with an applied hydrostatic stress of 240 MPa. It should be noted that the latter pressure was well above the alumina creep stress level, but only about half that for the silicon carbide creep tests. In addition to the six samples which received post-creep treatments, a single alumina sample was left in the as-crept condition to determine the repeatability of the SANS measurements. The post-creep thermal treatments employed for each sample are listed in Table 2. Following these treatments, the cavity distributions were again characterized by SANS as described above.

3. RESULTS

At the present time there exists no precise method to define the degree of damage based on a knowledge of the cavitation state. Nonetheless, it is possible to identify a number of parameters upon which the damage state should depend. If we confine ourselves to the early stages of creep, which is the regime where SANS is most effective, damage accumulation is truly a bulk phenomenon, and bulk parameters such as cavity density (number of cavities per unit volume) and volume fraction (total cavity volume per unit volume) should be of critical importance in defining damage. (During the intermediate and final stages of creep, local parameters such as the size of the largest cavity or cavity cluster, or the average spacing within a cluster, may be more appropriate measures of damage.) Changes in the bulk cavitation parameters will therefore be stressed in the following section. Measurements of average cavity size will also be included for added insight.

It should be noted that assessing relative degrees of damage in various specimens is a process fraught with possible ambiguity. For example, the

cavitated volume may increase while cavity density decreases; this would certainly be accompanied by an increase in average cavity size ($\bar{R}$), as well as in the actual number of cavities of this size. On the other hand, suppose V_c/V decreases, and so does N_c/V; if the latter is accomplished principally by the sintering of the smaller cavities in the distribution, $\bar{R}$ will increase, while the number of such cavities will remain roughly constant, or even decrease. In

TABLE 3
Cavity Parameters Calculated from the SANS Data

Sample number	*Sample condition*	$V_c/10^{-3}V$	$(N_c/V)/\mu m^3$	R_G/nm	R_p/nm
A-1	Crept	0·082 3	0·053 3	80·9	71·8
A-1	Crept and annealed without pressure	0·096 2	0·084 0	80·6	61·1
A-2	Crept	0·100	0·067 2	79·5	71·3
A-2	Crept and hipped (34 MPa)	0·131	0·118	80·3	54·6
A-3	Crept	0·155	0·181	79·6	55·8
A-3	Crept and hipped (240 MPa)	0·058 1	0·036 2	87·8	71·1
A-4	Crept	0·090 5	0·085 4	80·8	63·4
A-4	Crept	0·091 0	0·085 2	81·6	63·4
S-1	Crept	6·49	9·85	72·4	57·6
S-1	Crept and annealed without pressure	5·60	16·1	67·5	42·1
S-2	Crept	4·85	5·38	73·2	64·3
S-2	Crept and hipped (34 MPa)	4·03	8·55	68·6	42·1
S-3	Crept	1·89	4·61	74·4	47·5
S-3	Crept and hipped (240 MPa)	1·65	5·12	71·9	42·0

the first case cited, an increase in $\bar{R}$ reflects a real increase in cavitated volume, while in the second, it does not. In a similar manner, a decrease in $\bar{R}$ would represent an increase in either the actual, or the relative, number of small cavities present.

The results of the SANS measurements are listed in Table 3. The methods used for determining the cavity volume fraction, V_c/V, the cavity density, N_c/V, the radius of gyration, R_G, and the Porod radius, R_p, are described in the Appendix.

3.1. Data repeatability

As mentioned in Section 2, specimen A-4 was employed to check the repeatability of the SANS results. This sample's cavity distribution was originally measured together with the other as-crept samples and then remeasured, without undergoing any post-creep treatment, with the hipped specimens. Comparison of the results of the two separate measurements of specimen A-4 indicates that the SANS measurements are indeed highly repeatable; maximum variation between the two sets of measurements was less than 1 %.

3.2. Post-creep treatment of sintered alumina

As shown in Table 3, thermal treatment of the alumina for 24 h at 1600 °C in the absence of a hydrostatic pressure did not remove, and in fact actually increased, cavity damage, resulting in a 16 % increase in the cavity volume fraction, a 58 % increase in the cavity density, a 15 % decrease in R_p, and no change in R_G. The use of a hydrostatic pressure of 34 MPa worsened the damage state still further, yielding a 31 % increase in cavity volume fraction, a 75 % increase in cavity density, and a 23 % decrease in R_p. Application of a hydrostatic pressure of 240 MPa, on the other hand, resulted in a dramatic reduction in both the cavity density and volume fraction; after 4 h at 240 MPa, the cavity density and volume fraction had decreased by 80 and 63 %, respectively. This decrease resulted in a cavity density and volume fraction substantially below that present prior to creep.

Cavity size distributions for the alumina samples are presented in Fig. 1. These distributions clearly show the increase in total cavity number which occurred upon either pressureless annealing or low pressure hipping, Fig. 1(a) and (b). It also is evident that the largest increase occurred near the peak of the distributions. Thus, the observed decrease in R_p was the result of an actual increase in the number of smaller cavities, rather than a decrease in the number of larger cavities through sintering. The distributions in Fig. 1(c), on the other hand, clearly show the reduction in cavity density brought about by higher pressure hipping; a slight shift of the distribution toward larger diameters is also apparent. In combination, these observations suggest that removal of the smaller cavities occurred more efficiently, and also that growth of some of the largest cavities had occurred.

3.3. Post-creep treatment of hot-pressed silicon carbide

Thermal treatment of the silicon carbide for 24 h at 1600 °C in the absence of a hydrostatic pressure provided mixed results (Table 3); the cavity volume

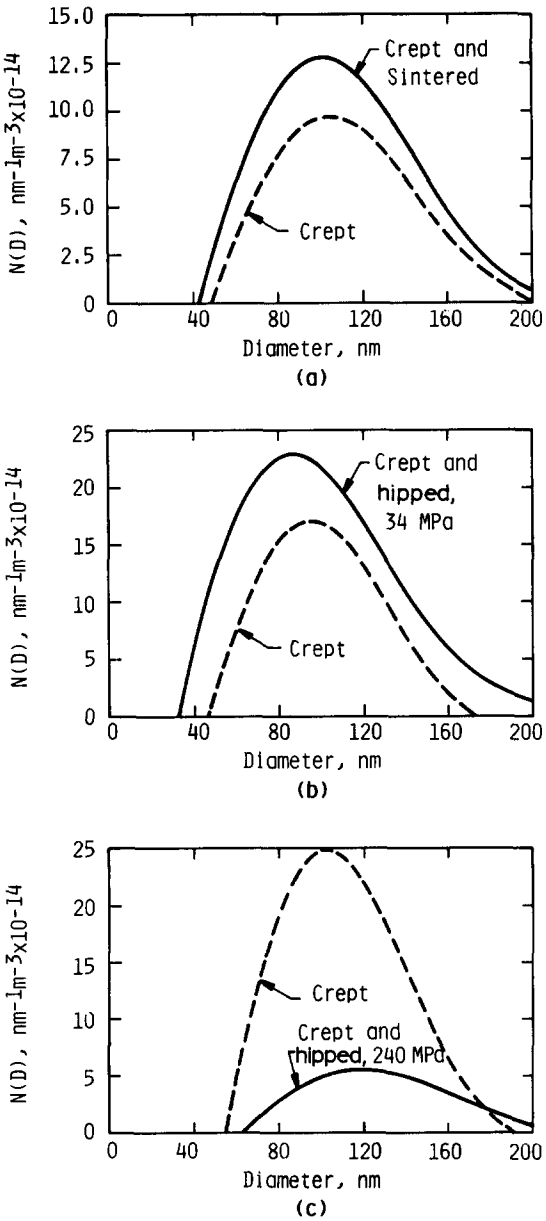

Fig. 1. Cavity size distributions for alumina specimens before and after post-creep treatment, illustrating the effect of (a) annealing without pressure, (b) hipping at 34 MPa, and (c) hipping at 240 MPa.

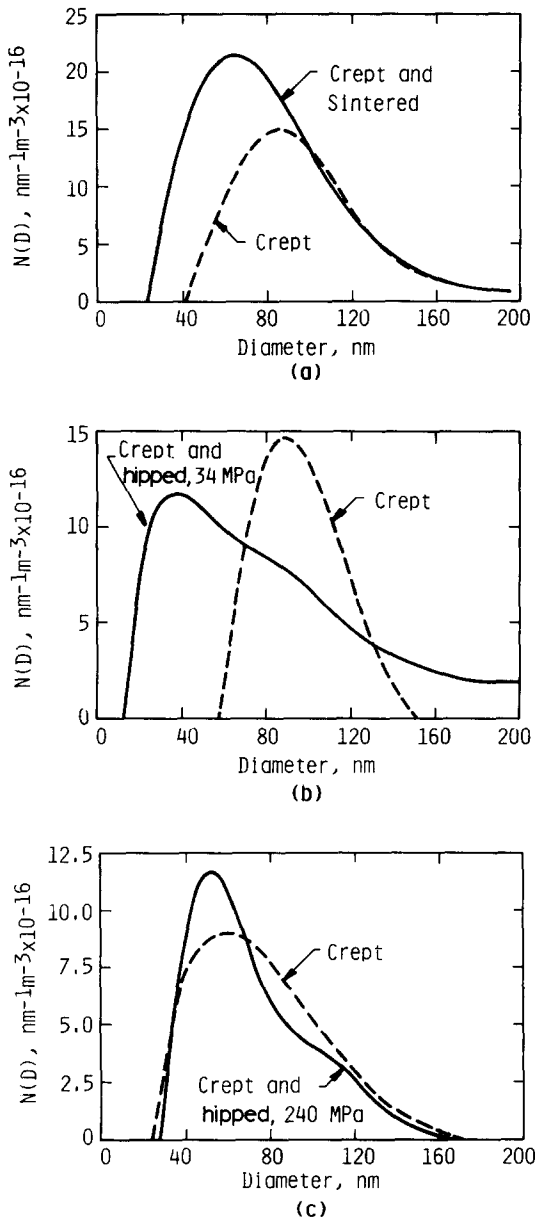

Fig. 2. Cavity size distributions for silicon carbide specimens before and after post-creep treatment, illustrating the effect of (a) annealing without pressure, (b) hipping at 34 MPa, and (c) hipping at 240 MPa.

fraction, R_G, and R_p decreased by 14, 7, and 27%, respectively, while the cavity density increased by 64%. Thermal treatment with a moderate hydrostatic pressure (34 MPa) yielded results very similar to those obtained with no pressure; cavity volume fraction, R_G, and R_p decreased by 17, 6, and 35%, respectively and cavity density increased by almost 59%. Application of a relatively high hydrostatic pressure resulted in a 15% decrease in cavity volume fraction, a slight decrease in R_G and R_p, and a 10% increase in cavity density.

Cavity size distributions for the silicon carbide samples are presented in Fig. 2. Comparison of the size distributions obtained following creep with those following the post-creep thermal treatments, Fig. 2(a), indicates that the increase in cavity density which occurred during thermal treatment was the result of the formation of additional cavities ranging from 20 to 100 nm in diameter. The number of cavities larger than 100 nm in diameter remained essentially constant during thermal treatment. The evolution of the cavity distribution during the low pressure hipping, Fig. 2(b), was considerably more complex. The number of small (≤ 60 nm) and large (≥ 130 nm) cavities and the total number of cavities increased, while the number of cavities between 60 nm and 130 nm decreased. This behavior suggests that three processes—cavity sintering, cavity growth and cavity nucleation—occurred simultaneously. Hipping at the higher pressure eliminated most, if not all, of the cavity nucleation and growth observed at the lower pressure. The only significant alteration of the cavity distribution upon hipping at 240 MPa, Fig. 2(c), was a reduction in the number of intermediate sized cavities (70–110 nm), and a subsequent increase in the number of small cavities (< 70 nm) which, most likely, occurred through sintering.

4. DISCUSSION

The results presented above indicate that removal of prior creep damage in the form of grain boundary cavitation is possible if the proper combination of time, temperature, and hydrostatic pressure is employed. This is clearly demonstrated by the response of the alumina hipped at 1600°C and 240 MPa. Four hours of this pressure/temperature combination reduced the cavitation level to a point below that present prior to creep. However, the results also suggest that the wrong choice of conditions can lead to increased, rather than decreased, damage levels. An increased damage level was quite obvious in the alumina samples that were annealed with no applied pressure, or hipped at 34 MPa. In both instances the cavity density and volume fraction increased as a result of the thermal treatment. An increased

damage level also probably occurred in the silicon carbide samples that were annealed with no applied pressure or hipped at 34 MPa. Although the cavity volume fraction decreased slightly, the cavity density increased dramatically during treatment. It is therefore important that a judicious choice of treatment conditions be made.

The observed removal of cavities during the 240 MPa hipping of sintered alumina is entirely consistent with our present understanding of cavity growth/sintering and, therefore, requires no further discussion. The nucleation of cavities observed during pressureless annealing and hipping (34 MPa) of both alumina and silicon carbide, however, deserves additional comment. The obvious question that comes to mind is whether the nucleation of cavities, as identified by SANS, could be an artifact of the measurement technique. Previous studies[11,12] have shown that the two materials included in this study are microstructurally stable at 1600 °C and, additionally, have demonstrated quite good correlation between SANS-generated cavitation parameters and similar parameters obtained independently by electron microscopy and precision density measurements. It thus can be concluded that the SANS measurements are truly indicative of an increase in the number of cavities of approximately 100 nm or less in radius. An obvious alternative to the proposed nucleation would be the shift of cavities from above, to below, the upper SANS detection limit, thus increasing the number of cavities detected, but with no actual increase in the number present. A simple calculation performed for sample S-1 indicates that if the additional cavities, which number 9·77 μm^{-3}, were the result of the shrinkage of cavities from slightly above ($R \approx 100$ nm) to slightly below ($R \approx 75$ nm) the upper detection limit, then a net density change of 2·4 % would occur. Although a density change of this magnitude would be easily detectable, precision density measurements performed before and after the thermal treatments showed no measurable change. Thus, it is apparent that the measured cavity increase could not have come from the sintering of larger cavities and, therefore, must have resulted from cavity nucleation, as postulated.

The most logical explanation of cavity nucleation during thermal treatment centers around the presence of local residual stresses which were either locked in following the creep loading, or induced by local rearrangements during treatment. Residual microstresses have been shown to nucleate cavities in metals during subsequent annealing,[14-16] and a similar process could be operating in the ceramic materials of this study. At this point, however, such arguments are purely speculative. Additional work is needed to identify the mechanism of cavity nucleation in ceramics during thermal annealing.

One can also speculate as to the reasons for the absence of significant

cavity shrinkage during most of the thermal treatments. Similar results have been obtained by Stevens and Flewitt[17] in a nickel–2 % chromium alloy. The presence of an internal gas pressure is one possible means of balancing the surface tension and thus inhibiting cavity shrinkage. However, we doubt that this is the present case. An alternative, and more reasonable explanation for the lack of sintering, can be obtained from the concepts of matrix constraint. As pointed out by Raj and Ghosh,[18] cavity growth in a polycrystalline material can be constrained by the surrounding uncavitated material. In this situation the cavity growth rate is controlled by the bulk creep rate. Since the creep rates at 1600 °C and zero (or low) applied pressure should be near zero, it is likely that matrix constraint severely inhibits cavity sintering. If matrix constraint is indeed important, one would expect significant cavity shrinkage rates only at high hydrostatic pressures, which could produce significant matrix creep, as was observed for the alumina sample hipped at 240 MPa. Conversely, 240 MPa is insufficient pressure to produce significant creep, and attendant cavity shrinkage, in the silicon carbide initially crept at 570 MPa. Higher stresses or temperatures thus would be needed for cavity removal in this material.

5. CONCLUSIONS

The following conclusions can be drawn from the results obtained in the present investigation:

1. Removal of creep damage, that is, grain boundary cavities, can be achieved at the creep temperature, provided a sufficient hipping stress is employed.
2. Reduction of the damage level occurs by a reduction in both the cavity volume fraction and the number of cavities.
3. Thermal treatments performed with insufficient hydrostatic pressure can lead to an increased damage level, which occurs primarily through cavity nucleation during the thermal treatment.

ACKNOWLEDGEMENTS

The authors are grateful to the Department of Energy, Office of Basic Energy Sciences, for support of this work, under Grant No. DE-FG05-84ER45063. We also thank the staff of the National Center for Small-Angle Scattering Research for their assistance in this project.

APPENDIX

Standard methods for analyzing small-angle scattering data were used to determine the radius of gyration, R_G, the Porod radius, R_p, and the total cavity volume, V_c/V. The equations employed in the analyses are presented below. Reference 19 should be consulted for a more complete description of these methods, and for an explanation of scattering theory. References 11 and 12 should be consulted for a description of the subtraction techniques employed.

For the case of a dilute distribution of non-interacting scatterers the invariant is proportional to the total cavity volume as

$$\int_0^\infty \frac{d\Sigma}{d\Omega} q^2 \, dq = 2\pi^2 (\Delta\rho)^2 \frac{V_c}{V} \tag{A1}$$

where $d\Sigma/d\Omega$ is the macroscopic differential scattering cross-section and $\Delta\rho$ is the scattering length density difference between a cavity and the matrix. Since the measured data extended into both the Guinier and Porod regions, it was possible to extrapolate the scattering curves such that the q range from zero to infinity was covered, and thus permit evaluation of the invariant.

The Porod radius was determined from

$$R_p = \frac{\frac{3}{\pi} \int_0^\infty q^2 \frac{d\Sigma}{d\Omega} dq}{\lim_{q \to \infty} q^4 \frac{d\Sigma}{d\Omega}} \tag{A2}$$

In eqn (A2) the Porod radius is equal to $\langle R^3 \rangle / \langle R^2 \rangle$, where R is the void radius and $\langle \ \rangle$ denotes an average over the ensemble.

A second measure of the size of the pores, the radius of gyration, was calculated from the slope of $\ln(d\Sigma/d\Omega)$ vs q^2 in the Guinier region as

$$\ln \frac{d\Sigma}{d\Omega} = A - \frac{R_G^2}{3} q^2 \tag{A3}$$

For spherical scatterers, the square of the radius of gyration is equal to $3\langle R^8 \rangle / 5\langle R^6 \rangle$. Hence, both R_p and R_G are moments which lie toward the high end of the size distribution.

Cavity size distributions were obtained from the SANS data by the transformation method developed by Letcher and Schmidt[20] and Fedorova and Schmidt.[21] For the case of single scattering from spherical pores the number density function, $N(D)$, is given by

$$N(D) = \frac{1}{D^2} \int_0^\infty \left[q^2 \frac{d\Sigma}{d\Omega}(q) - C_4 \right] \phi(qD) \, dq \tag{A4}$$

where

$$\phi(x) = \cos 2x\left[1 - \frac{2}{x^2}\right] - \frac{2\sin 2x}{x}\left[1 - \frac{1}{2x^2}\right] \tag{A5}$$

and C_4 is the Porod constant. Equation (A4) was numerically evaluated using the measured $d\Sigma/d\Omega$ values over the q range available and extrapolating the $d\Sigma/d\Omega$ values in the high q regime by the method developed by Brill and Schmidt,[22] and by the Guinier approximation in the low q regime. Absolute values of $N(D)$ were obtained by normalizing with respect to the total surface area determined independently from the Porod constant.

The number of cavities per unit volume, N_c/V, was obtained by integrating the absolute number density function with respect to D, the cavity diameter.

$$\frac{N_c}{V} = \int_0^\infty N(D)\,dD \tag{A6}$$

REFERENCES

1. Evans, A. G. and Rana, A., High temperature failure mechanisms in ceramics, *Acta Met.*, **28** (1980) 129–41.
2. Hull, D. and Rimmer, D. E., The growth of grain boundary voids under stress, *Phil. Mag.*, **4** (1959) 673–89.
3. Raj, R. and Dang, C. H., De-adhesion by the growth of penny-shaped bubbles in an adhesive layer, *Phil. Mag.*, **32** (1975) 909–22.
4. Hendricks, R. W., Schelten, J. and Schmatz, W., Studies of voids in neutron-irradiated aluminum single crystals—II. Small angle neutron scattering, *Phil. Mag.*, **30** (1974) 819–37.
5. Saegusa, T., Weertman, J. R., Cohen, J. B. and Roth, M., Small-angle neutron scattering from pores produced in high-temperature fatigue, *J. Appl. Cryst.*, **11** (1978) 602–4.
6. Kettunen, P. O., Lepisto, T., Kostorz, G. and Goltz, G., Voids produced by fatigue in copper single crystals of ⟨111⟩-orientation, *Acta Met.*, **29** (1981) 969–72.
7. Page, R. A., Weertman, J. R. and Roth, M., Small-angle neutron scattering study of fatigue induced grain boundary cavities, *Acta Met.*, **30** (1982) 1357–66.
8. Yoo, M. H., Ogle, J. C., Borie, B. S., Lee, E. H. and Hendricks, R. W., Small-angle neutron scattering study of fatigue induced cavities in nickel, *Acta Met.*, **30** (1982) 1733–42.
9. Cabanas-Moreno, J. G., Yang, M. S., Weertman, J. R., Roth, M., Zhang, Z. H., Wignall, G. D. and Koehler, W. C., Studies of grain boundary cavitation by small-angle neutron scattering, in *Fatigue Mechanisms: Advances in Quantitative Measurement of Physical Damage*, ASTM STP 811, Eds J.

Lankford, D. L. Davidson, W. L. Morris and R. P. Wei, ASTM, Philadelphia, 1983, 95–114.
10. Page, R. A. and Lankford, J., Characterization of creep cavitation by small-angle neutron scattering, *J. Am. Ceram. Soc.*, **66** (1983) C-146–8.
11. Page, R. A., Lankford, J. and Spooner, S., Small-angle neutron scattering study of creep cavity nucleation and growth in sintered alumina, *J. Mat. Sci.*, **19** (1984) 3360–74.
12. Page, R. A., Lankford, J. and Spooner, S., Nucleation and early-stage growth of creep cavities in hot-pressed silicon carbide, *Acta Met.*, **32** (1984) 1275–86.
13. Koehler, W. C. and Hendricks, R. W., The United States national small-angle neutron scattering facility, *J. Appl. Phys.*, **50** (1979) 1951.
14. Dyson, B. F., Profuse decohesion at grain boundaries in nimonic 80A, *Can. Met. Quart.*, **13** (1974) 237–43.
15. Dyson, B. F. and Rodgers, M. J., Prestrain, cavitation, and creep ductility, *Metal Sci.*, **8** (1974) 261–6.
16. Saegusa, T., Uemura, M. and Weertman, J. R., Grain boundary void nucleation in astroloy produced by room temperature deformation and anneal, *Met. Trans.*, **11A** (1980) 1453–8.
17. Stevens, R. A. and Flewitt, P. E. J., The role of hydrostatic pressure on the sintering of creep cavities in a nickel–2 % chromium alloy, *Acta Met.*, **27** (1979) 67–77.
18. Raj, R. and Ghosh, A. K., Stress rupture, *Met. Trans.*, **12A** (1981) 1291–302.
19. Weertman, J. R., Identification by small-angle neutron scattering of microstructural changes in metals and alloys, in *Nondestructive Evaluation: Microstructural Characterization and Reliability Strategies*, Eds. O. Buck and S. M. Wolf, AIME, New York, 1981, 147–68.
20. Letcher, J. H. and Schmidt, P. W., Small-angle X-ray scattering determination of particle-diameter distributions in polydisperse suspensions of spherical particles, *J. Appl. Phys.*, **37** (1966) 649–55.
21. Fedorova, I. S. and Schmidt, P. W., A general analytical method for calculating particle-dimension distributions from scattering data, *J. Appl. Crystallogr.*, **11** (1978) 405–11.
22. Brill, O. L. and Schmidt, P. W., Small-angle X-ray-scattering determination of diameter distributions, *J. Appl. Phys.*, **39** (1968) 2274–81.

Received 17 January 1986; accepted 26 March 1986